frontiers | Frontiers in Drug Delivery

TYPE Original Research
PUBLISHED 28 November 2022
DOI 10.3389/fddev.2022.1025029

OPEN ACCESS

EDITED BY
Arto Urtti,
University of Helsinki, Finland

REVIEWED BY
Vrinda Gote,
Inventprise Inc., United States
Marta Vicario-de-la-Torre,
Complutense University of Madrid, Spain

*CORRESPONDENCE
Sahar Awwad,
s.awwad@ucl.ac.uk
Yann Bouremel,
y.bouremel@ucl.ac.uk

SPECIALTY SECTION
This article was submitted to Ophthalmic Drug Delivery, a section of the journal Frontiers in Drug Delivery

RECEIVED 22 August 2022
ACCEPTED 18 October 2022
PUBLISHED 28 November 2022

CITATION
Liu T, Ibeanu N, Brocchini S, Khaw PT, Bouremel Y and Awwad S (2022), Development of an *in vitro* model to estimate mass transfer from the anterior cavity.
Front. Drug. Deliv. 2:1025029.
doi: 10.3389/fddev.2022.1025029

Development of an *in vitro* model to estimate mass transfer from the anterior cavity

Tianyang Liu[1,2], Nkiruka Ibeanu[1,2,3], Steve Brocchini[1,2,3], Peng Tee Khaw[1,3], Yann Bouremel[1,2,3]* and Sahar Awwad[1,2,3]*

[1]Optceutics Ltd, London, United Kingdom, [2]UCL School of Pharmacy, London, United Kingdom, [3]National Institute for Health Research (NIHR), Biomedical Research Centre at Moorfields Eye Hospital NHS Foundation Trust and UCL Institute of Ophthalmology, London, United Kingdom

Knowledge of drug mass transfer from the anterior chamber *via* the iris-lens barrier has important implications for the development of front of the eye medicines that can also deliver drugs to the vitreous cavity. Here, the design and evaluation of a novel *in vitro* model that estimates anterior clearance (CL) kinetics is described. To mimic some aspects of the human eye to aid with pharmaceutical modelling, the model incorporated a simulation of aqueous inflow from the ciliary inlet at the physiological flow rate, two CL elimination pathways [anterior hyaloid pathway and retina choroid sclera (RCS) pathway], human cavity dimensions and use of simulated vitreous fluid (SVF). An eye movement platform that incorporated 3 different eye movements (smooth pursuit, microsaccadic and saccadic) was tested against the control (no movement) to observe any difference in anterior kinetics profile and drug convection to the posterior cavity. Both timolol and brimonidine injected in the intracameral space were evaluated in the new *in vitro* prototype. An initial release study with one selected eye movement (smooth pursuit) with timolol (6.8 ± 0.4 µg, 30 µL) and brimonidine (15.3 ± 1.5 µg, 30 µL) showed half-life values of 105.3 and 97.8 min respectively in the anterior cavity (AC) space. Another study evaluated the effect of all eye movements against control with both drugs with higher doses of timolol (146.0 ± 39.1 µg, 25 µL) and brimonidine (134.5 ± 39.5 µg, 25 µL). The amounts of timolol in the back of the eye (RCS membrane and outflow) were 0.07 ± 0.05%, 1.36 ± 0.88%, 1.55 ± 1.03% and 0.98 ± 0.06% by 8 h with smooth pursuit, microsaccadic, saccadic and no movement respectively; whereas brimonidine amounts were 0.70 ± 0.21%, 0.94 ± 0.40%, 1.48 ± 1.02%, and 0.76 ± 0.33% respectively. A small amount of both drugs was seen in other compartments in the model (lens part, iris part, hyaloid membrane part and silicone cornea). These results indicate that this model can be used to determine transfer of small molecules *via* the iris-lens barrier to help optimise front of the eye formulations to treat tissues further back in the eye.

KEYWORDS

ocular, drug delivery, intracameral, small molecules, pharmaceutical modelling, ophthalmology

Introduction

Considerable efforts are being made to reduce vision loss, which is becoming more prevalent with an increasingly ageing population. Approximately 285 million people are visually impaired with 90% of these people living in developing countries (Bastawrous et al., 2014; Burton et al., 2021). In the last couple of decades, there has been considerable progress in the development of novel anti-vascular endothelial growth factor (VEGF) therapies, ocular hypotensive treatment therapy, and treatments of ocular surface disease (Gu and Janetos, 2021). Although there has been an increase in the number of therapies with an increase in Research & Development (R&D) capabilities and expenditures, the first decade of the century saw an overall average yearly decrease in new molecular entity and biologic approvals (Kaitin and Dimasi, 2011; Hay et al., 2014). Unbalanced regulatory risk-benefit assessments and efficacy hurdles with an increased complexity, and cost of clinical trials have contributed to this dynamic (Hay et al., 2014). With an exponential increase in the ageing population, the ophthalmic market is growing rapidly, but still poses a challenge for human health and economic growth (Delplace et al., 2015).

Development of efficacious ocular medicines is challenging. The least invasive routes for ocular drug administration are topical (e.g., eyedrops) and systemic (e.g., tablets) formulations. Topical administration often displays limited bioavailability (<5%) (Schopf et al., 2015) due to physical and biochemical barriers (Awwad et al., 2017a) including the pre-corneal tear film, the structure and biophysiological properties of the cornea, the limited volume that can be accommodated by the cul-de-sac, the lacrimal drainage system and reflex tearing. Patient nonadherence to eyedrops includes difficulty and forgetfulness in instilling eyedrops (Shen et al., 2020). Other routes of administration, such as intracameral delivery directly into the anterior chamber, have been reported to reduce systemic and corneal side effects that commonly arise with topical eyedrop steroid therapy (Shah et al., 2018). For example, a bimatoprost implant is administered intracamerally for the reduction of intraocular pressure (IOP) between 4–6 months (Seal et al., 2019). More invasive therapies, such as intravitreal delivery by injection in the posterior segment poses higher risks to the eye, are commonly used to achieve higher therapeutic drug concentrations in the vitreous and retina. However, poor patient compliance and more severe side effects associated with repeated frequency of intravitreal injections (Jager et al., 2004) still make topical or intracameral delivery a preferred route of administration if appropriate drug concentrations can be achieved in the posterior segment.

There is a considerable global effort to deliver drugs from the anterior cavity into the vitreous cavity. Topical or intracameral delivery to the back of the eye would provide a breakthrough in the treatment of blinding conditions if successful (Schopf et al., 2015). It is important to achieve sufficient drug concentrations in the aqueous humour (AH) after anterior segment treatment to accurately determine ocular bioavailability (Fayyaz et al., 2020a). While majority of drugs administered topically or intracamerally will clear from the anterior chamber with the aqueous outflow, anterior segment formulations are still considered by many major companies to be potentially important adjunct therapies to treat intraocular conditions that could provide maintenance therapeutic concentrations, including supporting an initial loading dose delivered by an intravitreal injection. Such an approach becomes potentially feasible with drugs that are currently being developed. Developing front of the eye formulations for intravitreal drug distribution requires knowledge of drug permeation through the cornea and drug biodistribution from the anterior chamber into the back of the eye. There are several corneal permeation models that are used; however, there is currently no adequate aqueous mass transfer model of the human eye that can determine the biodistribution of drug from the anterior chamber to the posterior chamber, particularly after intracameral injection.

Optimal formulation design is critical to achieve this goal. Currently, companies rely on animal models to refine formulation and dosage of ocular treatments. While non-primates can be used for toxicology, differences in ocular anatomy, physiology and immune response make it challenging to determine pharmacokinetics (Laude et al., 2010; Awwad et al., 2020). *In vitro* testing, in particular dissolution testing, plays an important role in the pharmaceutical industry, drug product R&D, drug quality evaluation and assessment of generic drugs (Chi et al., 2019), and characterising new drug candidates (Kuentz, 2015). It is strongly required to determine *in vitro* and *in vivo* correlations (IVIVCs) of drugs and dosing regimens compliant with quality standards (Chi et al., 2019), and to aid in bioequivalence studies in relation to product scale-up (Adrianto et al., 2022). Over the years, there has been progress in developing *in vitro* models for the back of the eye, from evaluation of protein stability in simulated vitreous (Patel et al., 2015), and understanding the importance of eye movements (EyeMos system) (Loch et al., 2014; Auel et al., 2021) to evaluating release kinetics of small and large molecules under the effect of aqueous flow [PK-Eye™ model (Awwad et al., 2015; Awwad et al., 2017b; Egbu et al., 2018; Awwad et al., 2019) and its variants (Sapino et al., 2019; Thakur et al., 2020)]. Computational eye modelling has been used to evaluate drug distribution too (Yi et al., 2022); however, no *in vitro* model has been reported

yet for the evaluation of mass transfer from the anterior to the posterior cavity in the presence of intraocular aqueous flow.

Here, the design of a new PK-Eye™ prototype to estimate mass transfer from the anterior to the posterior cavity under aqueous outflow is reported. The PK-Eye™ is already effective for determining the clearance (CL) of molecules injected into the vitreous (Awwad et al., 2015). The model incorporates aqueous inflow from the ciliary inlet at the physiological flow rate, two simulated CL elimination pathways (Cunha-Vaz, 1997; Kim et al., 2006; Bakri et al., 2007; Shatz et al., 2016) i.e., anterior hyaloid pathway (mostly for proteins and soluble small molecules) and retina choroid sclera (RCS) pathway (soluble small molecules), human cavity dimensions and use of a simulated vitreous fluid (SVF). An eye movement platform that has been previously developed (Velentza-Almpani et al., 2022) incorporated 3 different eye movements (smooth pursuit, microsaccadic and saccadic) and these movements were compared against the control (no movement) to observe any difference in drug convection to the posterior cavity. The release kinetics and distribution profiles of two small molecules (timolol and brimonidine) were evaluated in the anterior cavity (intracameral space).

Materials

Timolol maleate and brimonidine tartrate were purchased from Merck Life Science Ltd. (United Kingdom) and Cambridge Bioscience (Cambridge, United Kingdom) respectively. Phosphate buffered saline (PBS) tablets, agar, ammonium acetate, and high performance liquid chromatography (HPLC) grade water and methanol were purchased from Sigma Aldrich (Gillingham, Dorset, United Kingdom). Visking dialysis membrane tubing (molecular weight cut-off, MWCO of 12–14 kDa) and dialysis tubing (MWCO of 50 kDa) were obtained from Medicell International Ltd. (London, United Kingdom) and VWR International Ltd. (United Kingdom) respectively. Sodium hyaluronate (HA, 1.5–1.8 mDa) was purchased from Lifecore Biomedical, LLC (Chaska, MN, United States). FLPG Plus, LineUp Flow EZ, LineUp LINK module, remote control system, flow units S PACKAGE bundle, LineUP SUPPLY kit, FEP tubing (1/16–254) and LineUP ADAPT module were purchased from Fluigent (Le Kremlin-Bicêtre, France). Form 3B complete package, Formlabs BioMed clear resin, Formlabs tough 2000 resin, Form 3 resin tank v2.1 and Form 3 build platform were purchased from Additive-X Ltd. (Ripon, United Kingdom). PIMag® Rotation stage, Ø 32 mm clear aperture, iron core 3-phase torque motor, incremental angle measuring system with sin/cos signal transmission, PIMag® motion controller for magnetic direct drives, extension cable for motor signals and MS D-Sub 15 (f) PI to D-Sub 9 (f) PIM 3m were purchased from Physik Instrumente (Bedford, United Kingdom).

Methods

General model setup

The models were printed using the BioMed clear resin, which is a USP class VI certified material for biocompatible applications using the 3D printer Form 3B. Each part was printed with no internal support to ensure the smoothness of the model. The models were assembled and each model was connected to a 345 mbar LineUp Flow EZ pump. The 1-1 set up of the model with the LineUp Flow EZ pump consisted of the buffer (PBS, pH 7.4), a flow unit (that monitored the system in flow rate), as well as 127 and 254 μm tubing for the connection. All the LineUp Flow EZ pumps were connected to the FLPG plus 2-bar pump, which was the pressure pump source. The microfluidic system was connected to the computer for pressure and flow control through the Fluigent All-in-One (A-i-O) program. The microfluidic system was connected to the flow inlet of the back and front ports (2.0 μL/min) and allowed to equilibrate at 37°C for 48 h before injection.

Three movements (smooth pursuit, microsaccadic and saccadic) were investigated with an in-house eye movement platform (Velentza-Almpani et al., 2022). Smooth pursuit settings were 20° in 1.8 s reaching a maximum velocity of 22°/s, stop for 50 ms (velocity of 0°/s), and moved back 20° at the same velocity to reach an angle of 0°. The model then moved back in the opposite direction with the same velocity and angle patterns. Microsaccadic movement corresponds to eye fixation. Microsaccadic settings had a rotation of approximately 0.4° that moved back and forth every 1.25 s. The velocity reached a maximum of 25 to 26°/s to cover 0.4° in 20 ms. The saccadic movement corresponds to a reading movement with the eye and had a setting of 2° in movement in 100 ms every 330 ms up to 8° before going back to 0° in 400 ms (beginning of the line). The velocity reached a maximum of 41°/s.

In vitro release studies

SVF was prepared by first dissolving HA (2.5 mg/ml, 60.0 mg) in distilled water (24.0 ml) at 60–70°C for about 10 min. Agar (1.0 mg/ml, 24.0 mg) was then dissolved in a separate beaker in distilled water (24.0 ml) at 80–90°C. HA and agar were stirred together at 60–70°C for another 10 min. The SVF was then allowed to cool down to room temperature (RT, ~20–22°C) and incubated in the fridge (4°C) overnight. Initial studies using low doses of timolol (6.8 ± 0.4 μg/30 μL) and brimonidine (15.3 ± 1.5 μg/30 μL) were investigated in the intracameral space *via* the silicone cornea into models containing SVF using smooth pursuit only. Higher doses were then injected of both timolol (146.0 ± 39.1 μg/25 μL) and brimonidine (134.5 ± 39.5 μg/25 μL) *via* the silicone cornea. The models were dismounted at each time point between

0.5 and 8.0 h. Each compartment was washed and recovery fractions were quantified by HPLC. Outflow samples (i.e., RCS outflow and AH outflow) were directly collected at each time point and analysed by HPLC. For the drug remnants in the anterior (remaining in the AC) and posterior (SVF/VH) cavities, the contents were gently emptied into HPLC vials and directly analysed by HPLC. The membranes, i.e., RCS membrane (12–14 kDa) and hyaloid membrane (50 kDa) were removed from the model, immersed in distilled water (2.0 ml) in a glass vial and vortexed for 5.0 min to remove all drug on the surfaces. The silicone cornea, the iris part and the lens part of the models were also removed, and each of them was washed with distilled water (1.0 ml) for 1.0–2.0 min before HPLC analysis. The summation of all compartments and outflow determined the drug recovery, and allowed a more accurate calculation of drug release.

HPLC quantification of timolol and brimonidine

All analyses for timolol and brimonidine were undertaken using an Agilent 1200 series HPLC (Agilent Technologies Inc., Santa Clara, CA, United States) equipped with Chemstation software (Agilent) and a Zorbax C18 eclipse plus, 5 µm, 4,6 mm × 250 mm column (Agilent, Wokingham, Berkshire, United Kingdom). Both timolol and brimonidine were analysed with an isocratic method of mobile phase A (ammonium acetate, 0.01 M, pH 5.0) and B (methanol) with a ratio of 60:40 v/v (A:B) and 80:20 v/v (A:B) respectively. Both had a run time of 15.0 min with an additional 1.0 min post wash time. Other parameters included an injection volume of 50 µL, flow rate of 1.0 ml/min and column temperature of 30°C. Wavelengths of 295 nm and 254 nm were used for detection of timolol and brimonidine respectively. Timolol (0.4–450 µg/ml) and brimonidine (1.0–260 µg/ml) showed a retention time of 7.3 and 6.1 min with an R^2 value of 0.9999 and 0.999 for their calibration curves respectively.

Data analysis

All results are presented as the mean and standard deviation (±STD), and data were plotted using Prism 7 and GraphPad software. Half-life ($t_{1/2}$) values were calculated according to the best fitting model in GraphPad. First-order kinetic rate constants (k) were derived from the mono-exponential curve and $t_{1/2}$ was calculated using the equation: $0.693/k$. The rate constants (k) of zero-order release profiles were calculated as concentration-time and $t_{1/2}$ was calculated from initial concentration [A] using $[A]/2k$. Data was post-processed using MATLAB_R2017B, MathWorks. The program automatically reads and assigns each data column to a variable and plots them along pre-defined axes.

Results

Design of the intracameral model

An initial prototype (labelled as "ciliary inlet model") (Velentza-Almpani et al., 2022) was used to study mass transfer from the anterior to the posterior cavity. Briefly, the model consisted of two main parts (posterior and anterior cavities) with a flow inlet in the ciliary side and drug injection ports in both cavities with a membrane in between the 2 cavities. Both cavities of the model were filled with PBS, pH 7.4. Models were connected to the pumps and were allowed to equilibrate for 48 h with PBS, pH 7.4 at 2.0 µL/min. Dexamethasone is a small molecule routinely used in ocular drug delivery for treatment of inflammation; it was initially chosen as a model drug to demonstrate proof-of-concept. Dexamethasone was injected (100 µL, 1.0 mg/ml) into the anterior cavity (intracameral space) of the model directly through the anterior outlet port (Supplementary Figure S1). Samples were collected from the anterior cavity *via* the outflow port to estimate drug concentration in the anterior outflow. Samples from the posterior cavity were obtained by taking an aliquot (100 µL) from that cavity and replacing it with PBS, pH 7.4 (100 µL). All samples were analysed by HPLC with an already optimised method for dexamethasone (Velentza-Almpani et al., 2022). Results from this experiment demonstrated a 30–40% drug loss with the prototype when drug was injected in the front of the model. Drug leakage was observed during injection into the model due to the initial anterior injection port length and the small volume of the anterior cavity (~0.2 ml). Issues detected were the pressure buildup due to the small space, which pushed the drug solution out during injection resulting in drug loss and poor drug recovery. In addition, constant sampling from the posterior cavity by manually tapping the back might alter the drug distribution environment and drug release profiles.

Another prototype of the model was designed in response to the results reported above (Figure 1). The anterior cavity composed of different layers that broadly mimic the iris part, cornea part (use of a silicone cornea) and a lens part (Figure 1A), which were all assembled together with the help of screws. To account for the drug loss seen previously, the front of the model was fitted with a silicone cornea (0.5 mm thickness) that pursed under pressure to recreate a 3.0 mm anterior chamber depth. Drugs were injected using a 30G needle into the intracameral space (anterior cavity) through the silicone cornea (Figure 1B). The silicone cornea self-sealed with no drug leakage after injection. Previous work (Bouremel et al., 2021) showed that model silicone corneas only leaked at a high pressure (>50 mmHg) when pierced with a 1.0 × 0.2 mm (length × width) incision. Drug CL occurs by two outflows present in the model, i.e., anterior hyaloid pathway (front) and the RCS pathway (back), and it has also been reported to clear *via* permeation to the iris and ciliary body (and then blood flow

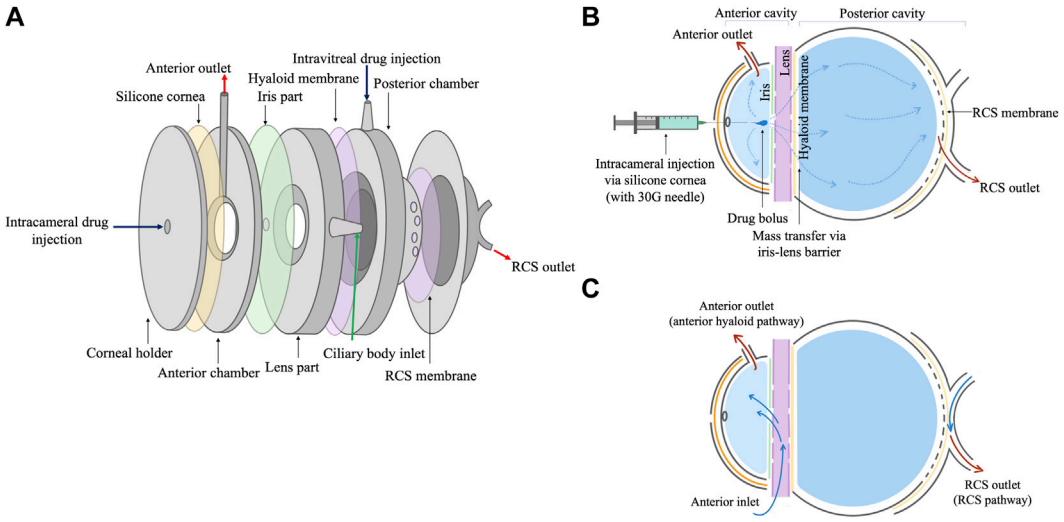

FIGURE 1
(A) Schematic of the design of the intracameral PK-Eye™ model showing each model compartment. Each part was screwed together to form the tight seal in the PK-Eye™ model. **(B)** Drug injection to the intracameral cavity *via* the silicone cornea using a 30G needle. **(C)** Schematic to demonstrate flow inlet and drug elimination from the model.

in these tissues) (Fayyaz et al., 2020b). The inflow and outflow ports were located at the ciliary inlet side/trabecular meshwork (TM) and in the anterior chamber respectively (Figure 1C). The hyaloid membrane in the model composed of a cellulose membrane with a MWCO of 50 kDa. The posterior cavity composed of a SVF with an inflow and outflow port located in the RCS part of the model. The RCS outflow and the membrane (12–14 kDa) were introduced to avoid manual tapping in the back of the eye, and to allow real-time sampling from that cavity. All models were connected to the microfluidic system after assembly to equilibrate the flow and pressure prior to the release kinetic experiments.

Eye movement platform

Eye movements were reproduced using the eye movement platform (Velentza-Almpani et al., 2022) by creating different convective motions (smooth pursuit, microsaccades and saccades). The three main movements of the eye are shown in Figure 2. For each movement, the velocity is shown in red and the position in black. Eye saccades lasted below 100 ms. The eye remained stationary between 200 and 400 ms between each saccade (Figures 2A). Once the models were mounted on the 3D printed platform and the rotation motor, the platform continuously moved by 2° in 100 ms followed by a rest period of 330 ms (Rayner, 1998). This motion was repeated 4 times to achieve a maximum of 8° followed by a movement back to the starting point, and again repeated continuously for a period of 8 h. The platform controlled the movement and adapted the velocity to achieve the required programming. When fixing on objects, the eye is not completely static but instead adopts small, jerky movements that are involuntary. When observing a blank scene, the rate of microsaccade is 0.8 Hz or 1 microsaccade every 1.25 s with a microsaccade magnitude of 0.43 ± 0.05° in 12.6 ± 0.1 ms. The platform loaded with 8 models was able to move by 0.4° (−0.2 to 0.2°) in 20 ms to recreate the fixation of a blank scene with a frequency of 0.8 Hz. In Figure 2B, the motor was able to move by 2° in 100 ms with very little jerky movement, and the program overshot to 2.055° before immediately correcting back to 2°. This was due to the momentum of the platform fully loaded with the 8 models. The eye overshot by 0.1° before decelerating to arrive at 0.2° (Figure 2B). The final movement corresponds to a smooth pursuit movement (Figure 2C). The smooth pursuit is a continuous voluntary movement of the eye without a break. It is reported that the eye can move up to 87°/s (Meyer et al., 1985) in a smooth pursuit movement with a common range speed between 20 and 40°/s (Larsby et al., 1988). This movement was reproduced with a first rotation from −20 to 0° then 0 to 20° before returning to −20° (Figure 2C). The platform did not have any jerky motion for a slow pursuit movement (Figure 2C).

In vitro studies

AH from the ciliary body flows at an approximate flow rate of 2.0 µL/min from the anterior chamber to the TM. Therefore, any drugs injected in the front of the eye will tend to quickly clear

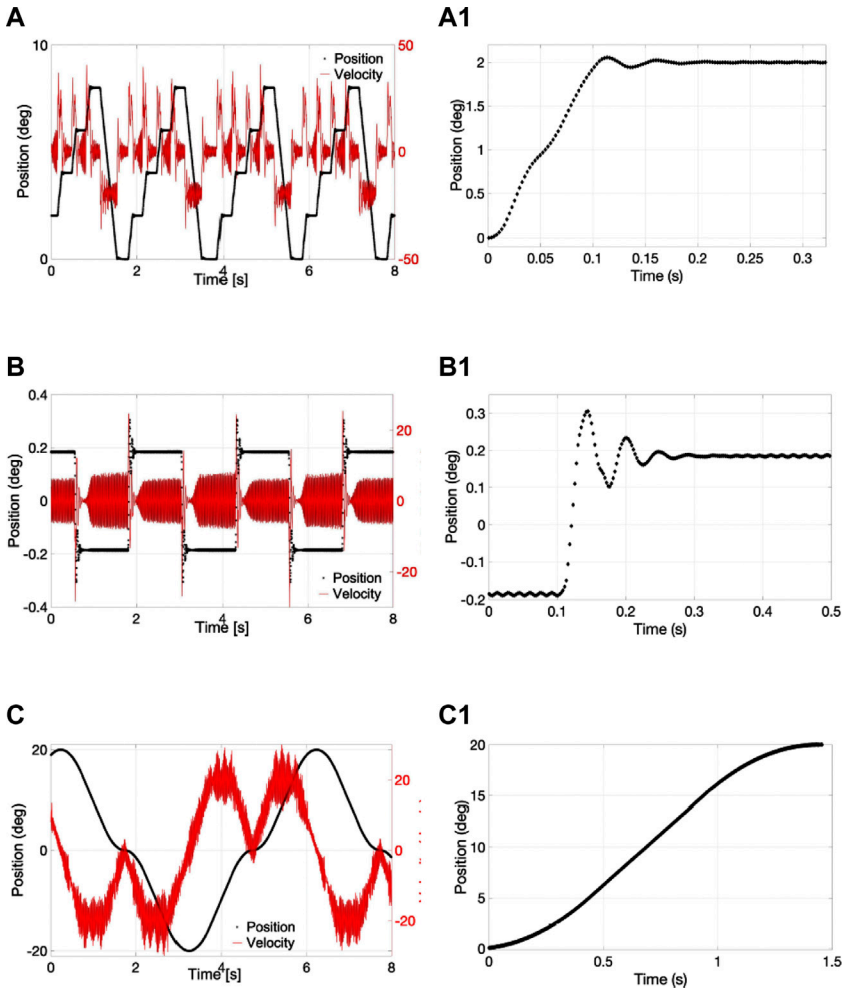

FIGURE 2
(A-A1) Saccadic, **(B-B1)** microsaccadic and **(C-C1)** smooth pursuit movement with the eye movement platform showing the **(A–C)** velocity and the position over 8 s and the **(A1-C1)** position from 0 to 2°, 0.2°, and 20° degrees respectively.

from the anterior chamber. Preliminary studies were first conducted with a low dose of timolol (6.8 ± 0.4 μg/30 μL) in the intracameral space using smooth pursuit movement and its release was analysed with HPLC. The low dose was initially chosen to compare the drug CL profiles to a study that was conducted in rabbit eyes with a similar dose injected in the intracameral space (Fayyaz et al., 2020a). At each time point, models were removed from the platform and amount of drug was calculated from the AH outflow, remnants in the anterior cavity, silicone cornea, iris part, lens part, hyaloid membrane, VH leftover, RCS membrane and RCS outflow (as highlighted in the methods section).

The amount of timolol seen remaining in the AC cavity, AH outflow, VH, RCS membrane and RCS outflow of the model by the 1.5-h time point were 59.2 ± 3.5%, 11.7 ± 2.1%, 24.0 ± 2.4%, 0.9 ± 0.3%, and 0.06 ± 0.03% respectively (Figure 3). AC cavity remnants and AH outflow showed higher drug concentrations as compared to other parts of the model, as majority of drug cleared from the front of the eye. Drug concentrations in the AC cavity, AH outflow, VH, RCS membrane and RCS outflow ranged from 2.0 to 4.0 μg/ml, 0.5–2.5 μg/ml, 0.3–0.5 μg/ml, 0.04–0.1 μg/ml and ~0.01 μg/ml respectively. In the other parts of the model, the amounts of timolol recovered from the lens part, iris part, hyaloid membrane and silicone cornea of the model were 1.5 ± 0.5%, 0.7 ± 0.05%, 1.7 ± 0.1% and 0.3 ± 0.2% respectively (Figure 4). Drug concentrations in these model compartments ranged from 0.05 to 0.2 μg/ml. The half-life of timolol (initial 6.8 ± 0.4 μg dose) in the AC cavity was calculated to be 105.3 min (k: 0.395 h^{-1}, R^2: 0.8000, Table 1). When compared to literature, the half-life of intracameral timolol (4.75 μg dose) in a study

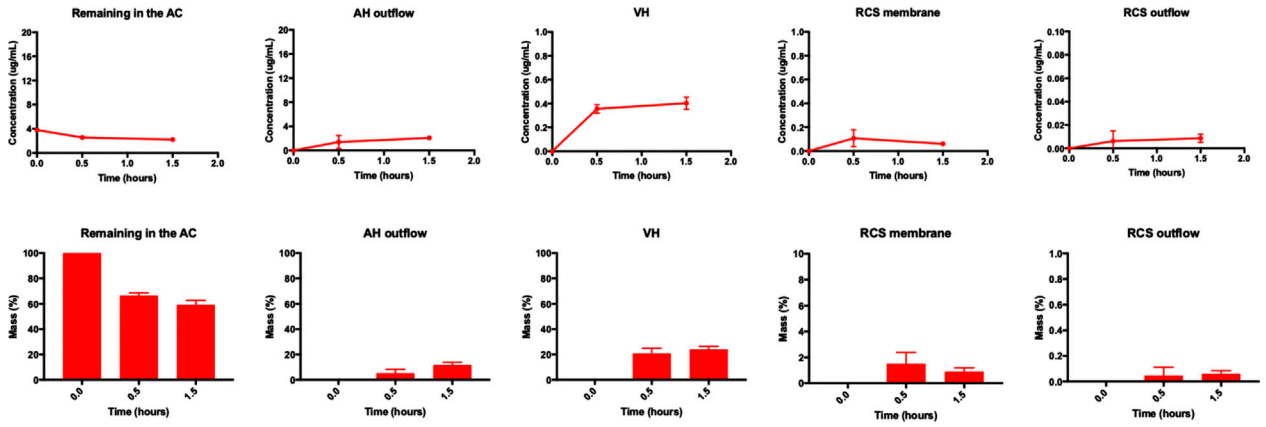

FIGURE 3
(top panel) Concentration profiles (μg/ml) and **(bottom panel)** mass profiles (%) of intracameral timolol (6.8 ± 0.4 μg) at various time points (0.0, 0.5, and 1.5 h) using smooth pursuit from the AC, AH outflow, VH, RCS membrane and RCS outflow of the model. All data are presented as the mean (n = 2) and standard deviation (±STD).

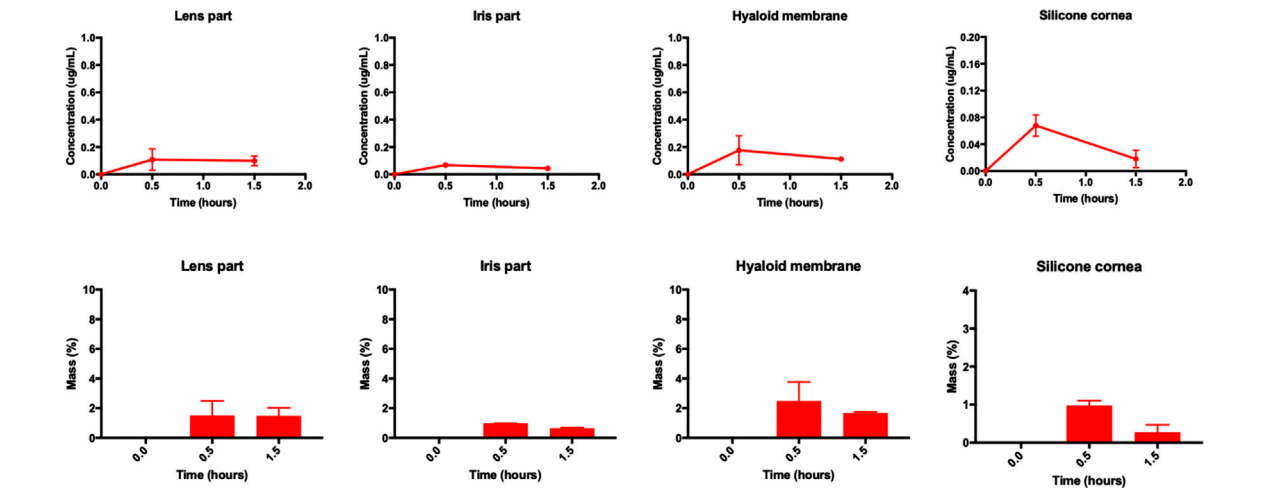

FIGURE 4
(top panel) Concentration profiles (μg/ml) and **(bottom panel)** mass profiles (%) of intracameral timolol (6.8 ± 0.4 μg) at various time points (0.0, 0.5, and 1.5 h) using smooth pursuit from the lens part, iris part, hyaloid membrane and silicone cornea of the model. All data are presented as the mean (n = 2) and standard deviation (±STD).

conducted in rabbits was reported to be 33.6 min (Fayyaz et al., 2020a), which is almost 3 × faster than what was observed in the model.

A higher dose of timolol (149.2 ± 46.7 μg/25 μL) was then injected in the intracameral space to investigate three types of eye movement (smooth pursuit, microsaccades and saccades) vs its control (no movement). A higher dose was chosen (almost 20 × the dose) to observe any significant change in half-life and drug CL properties. A similar dose of timolol (125 μg, 0.5% eye drop) was reported in another study that was conducted with topical timolol (Urtti et al., 1990). Interestingly, no significant differences in release profiles were seen in all experiments with and without movement, most probably as a result of the velocity and dominance of the physiological flow rate in the model in the anterior cavity (Figures 5, 6). Similar to the low dose study, the highest concentration was seen in the anterior cavity leftover (after the end of each study, ranging from 20.0 to 80.0 μg/ml) and the AH outflow i.e., before the front membrane (ranging

TABLE 1 Kinetic parameters of intracameral timolol and brimonidine from the PK-Eye™ model.

Drug	Dose (μg)	Model	Half-life (minutes)			
			Smooth pursuit	Microsaccadic	Saccadic	Control
Timolol	4.75	Rabbits	33.6 (Fayyaz et al., 2020a)			
	6.8 ± 0.4	PK-Eye™	105.3	-	-	-
	149.2 ± 46.7	PK-Eye™	265.9	146.0	302.6	210
Brimonidine	13.3	Rabbits	47.0 (del Amo et al., 2022)			
	15.3 ± 1.5	PK-Eye™	97.8	-	-	-
	134.5 ± 39.5	PK-Eye™	323.3	137.6	182.6	304.8

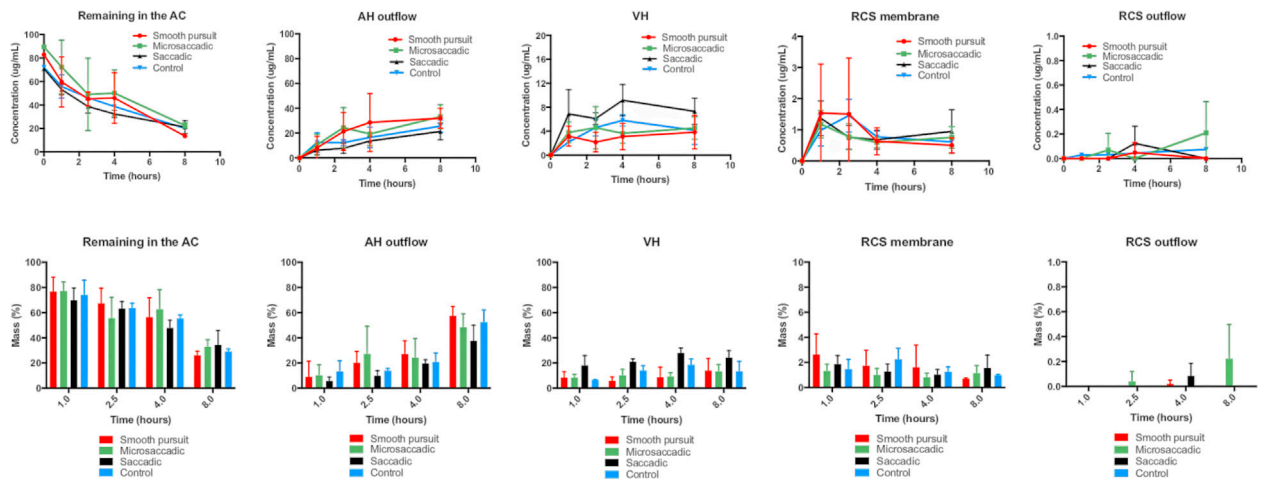

FIGURE 5
(top panel) Concentration profiles (μg/ml) and **(bottom panel)** mass profiles (%) of intracameral timolol (149.2 ± 46.7 μg) at various time points (1.0, 2.5, 4.0, and 8.0 h) using three movements: **(red)** smooth pursuit, **(green)** microsaccadic movement, **(black)** saccadic movement and **(blue)** control (no movement) from the AC, AH outflow, VH, RCS membrane and RCS outflow of the model. All data are presented as the mean (n = 4) and standard deviation (±STD).

from 10.0 to 40.0 μg/ml) (Figure 5). Comparable amounts of timolol were seen in the lens part (1.0–5.0 μg/ml), iris part (0.5–3.0 μg/ml) and hyaloid membrane (4.0–10.0 μg/ml). Timolol passed the iris-lens barrier (50 kDa) into the VH (5.0–2.0 μg/ml), RCS membrane (i.e., back membrane, <2.0 μg/ml) and RCS outflow (<0.2 μg/ml). By the 8-h time point, approximately 30% of the drug remained in the intracameral space (anterior leftover) with almost 45% of the drug seen to exit *via* the AH outflow (Figure 6). Timolol amounts seen in the back of the eye (*via* the RCS outflow and RCS membrane) by the 2.5-h time point were 1.73 ± 1.23%, 1.04 ± 0.48%, 1.28 ± 0.59%, 2.24 ± 0.88% whereas by the 8-h time point the amounts were 0.07 ± 0.05%, 1.36 ± 0.88%, 1.55 ± 1.03%, and 0.98 ± 0.06% with smooth pursuit, microsaccadic, saccadic and no movement respectively. Approximately 1–2% of timolol was quantified in all other compartments (except AC cavity, AH outflow and VH) for all movements and control (Figure 6). The half-lives of timolol in the AC cavity with smooth pursuit, microsaccades, saccades and control were 265.9 min (k: 0.1564 h^{-1}, R^2: 0.8232), 146.0 min (k: 0.2848 h^{-1}, R^2: 0.5793), 302.6 min (k: 0.1374 h^{-1}, R^2: 0.8066) and 210.4 min (k: 0.1976, R^2: 0.8401) respectively (Table 1).

Preliminary studies were also conducted with low dose brimonidine (15.3 ± 1.5 μg/30 μL) in the intracameral space using smooth pursuit movement. The dose was chosen to compare the release kinetics to a study conducted in rabbit eyes using a similar dose (13.3 μg) of intracameral brimonidine (del Amo et al., 2022). Similar trends in release profiles seen with low dose timolol were also seen with low dose brimonidine. The amounts of

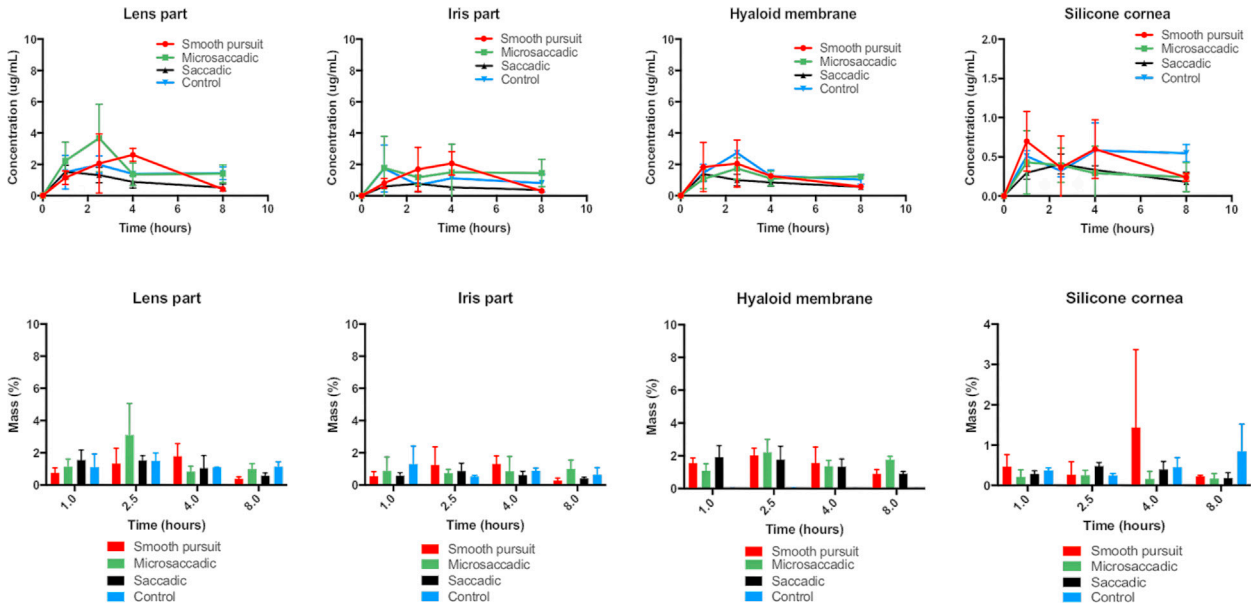

FIGURE 6
(top panel) Concentration profiles (μg/ml) and **(bottom panel)** mass profiles (%) of intracameral timolol (149.2 ± 46.7 μg) at various time points (1.0, 2.5, 4.0, and 8.0 h) using three movements: **(red)** smooth pursuit, **(green)** microsaccadic movement, **(black)** saccadic movement and **(blue)** control (no movement) from the lens part, iris part, hyaloid membrane and silicone cornea of the model. All data are presented as the mean (n = 4) and standard deviation (±STD).

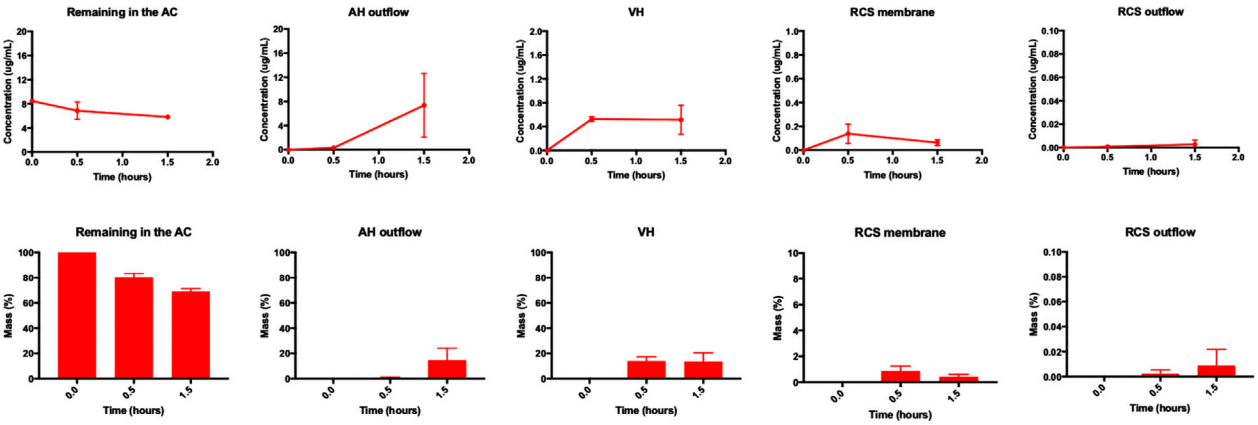

FIGURE 7
(top panel) Concentration profiles (μg/ml) and **(bottom panel)** mass profiles (%) of intracameral brimonidine (15.3 ± 1.5 μg) at various time points (0.0, 0.5, and 1.5 h) using smooth pursuit from the AC, AH outflow, VH, RCS membrane and RCS outflow of the model. All data are presented as the mean (n = 2) and standard deviation (±STD).

brimonidine seen in the AC cavity, AH outflow, VH, RCS membrane and RCS outflow of the model by the 1.5-h time point were 69.0 ± 2.2%, 14.6 ± 9.6%, 13.7 ± 6.9%, 0.4 ± 0.2%, and 0.010 ± 0.009% respectively (Figure 7). Drug concentrations in the AC cavity, AH outflow, VH, RCS membrane and RCS outflow ranged from 5.5 to 8.5 μg/ml, 0.1–10.0 μg/ml, 0.3–0.7 μg/ml, 0.05–0.2 μg/ml and 0.001 μg/ml respectively. In the other parts of the model, the amounts of timolol recovered from the lens part, iris

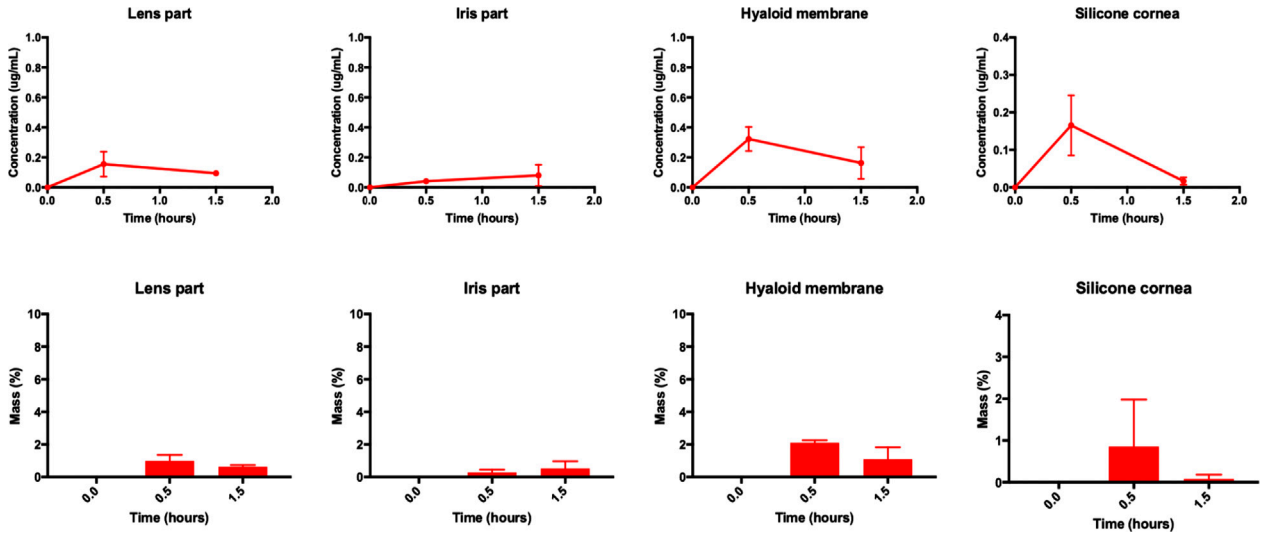

FIGURE 8
(top panel) Concentration profiles (μg/ml) and **(bottom panel)** mass profiles (%) of intracameral brimonidine (15.3 ± 1.5 μg) at various time points (0.0, 0.5, and 1.5 h) using smooth pursuit from the lens part, iris part, hyaloid membrane and silicone cornea of the model. All data are presented as the mean (n = 2) and standard deviation (±STD).

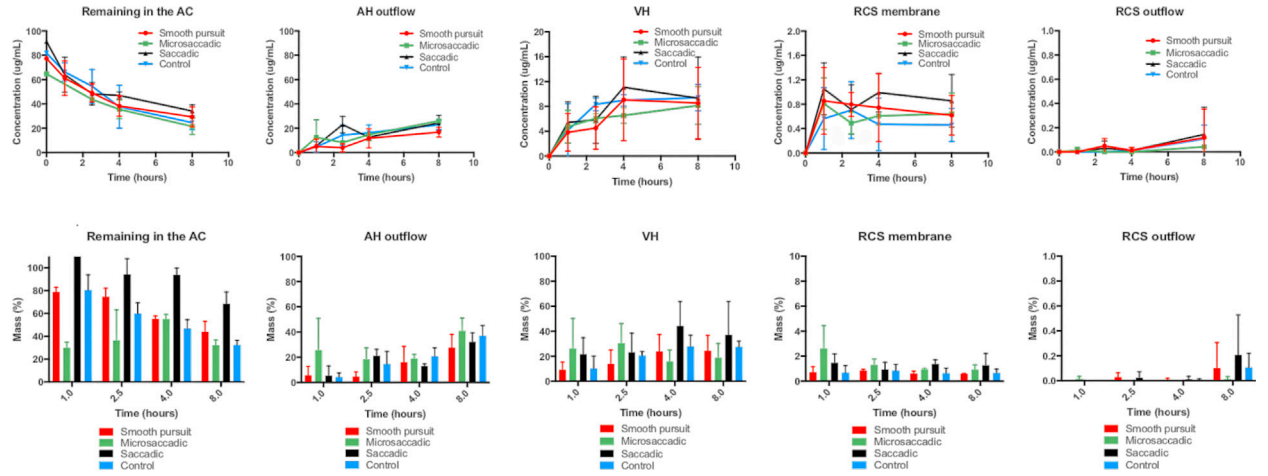

FIGURE 9
(top panel) Concentration profiles (μg/ml) and **(bottom panel)** mass profiles (%) of intracameral brimonidine (134.5 ± 39.5 μg) at various time points (1.0, 2.5, 4.0, and 8.0 h) using three movements: **(red)** smooth pursuit, **(green)** microsaccadic movement, **(black)** saccadic movement and **(blue)** control (no movement) from the AC, AH outflow, VH, RCS membrane and RCS outflow of the model. All data are presented as the mean (n = 4) and standard deviation (±STD).

part, hyaloid membrane and silicone cornea of the model were 0.6 ± 0.1%, 0.5 ± 0.4%, 1.1 ± 0.7% and 0.10 ± 0.08% respectively (Figure 8). The half-life of brimonidine (15.3 ± 1.5 μg initial dose) in the AC cavity was calculated to be 97.8 min (k: 0.4265 h^{-1}, R^2: 0.9849, Table 1). In a study conducted in rabbits, the half-life of intracameral brimonidine (13.3 μg dose) was reported to be 47.0 min (del Amo et al., 2022), which is approximately 2 × faster than what was observed in the model.

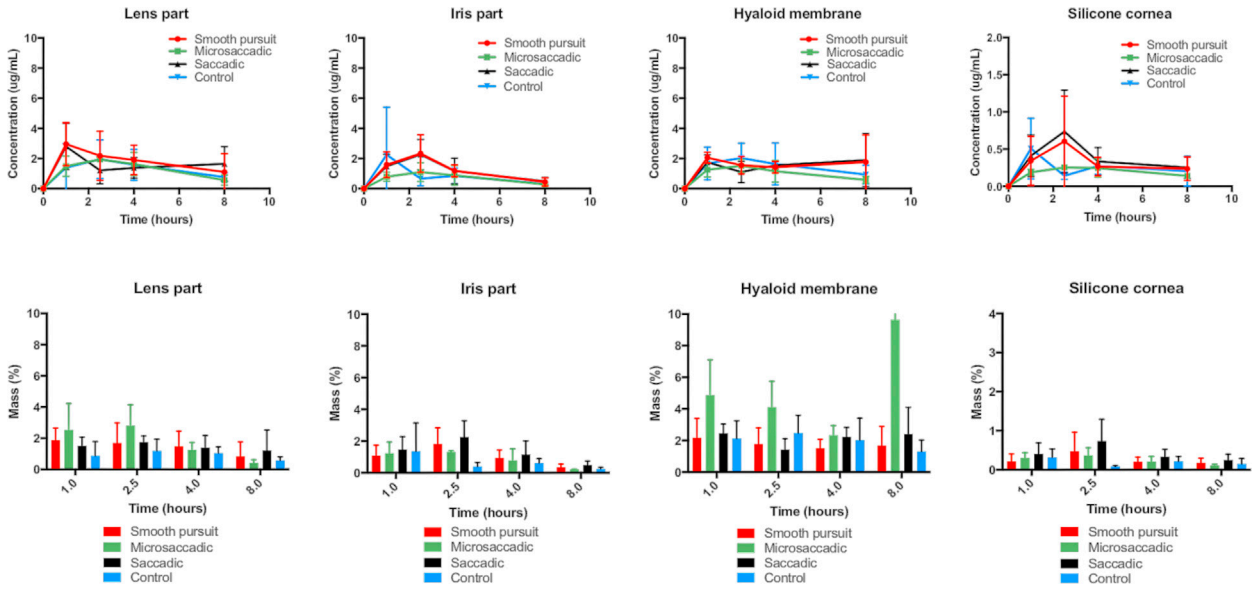

FIGURE 10
(top panel) Concentration profiles (μg/ml) and **(bottom panel)** mass profiles (%) of intracameral brimonidine (134.5 ± 39.5 μg) at various time points (1.0, 2.5, 4.0 and 8.0 h) using three movements: **(red)** smooth pursuit, **(green)** microsaccadic movement, **(black)** saccadic movement and **(blue)** control (no movement) from the lens part, iris part, hyaloid membrane and silicone cornea of the model. All data are presented as the mean (n = 4) and standard deviation (±STD).

Brimonidine (134.5 ± 39.5 μg, 25 μL) was also injected in the intracameral space and its release was investigated with three movements and its control (no movement) for both its concentration (Figure 9) and mass (Figure 10) profiles. The dose chosen was similar to topical brimonidine (119 μg) that was tested in rabbit eyes in another study (Acheampong et al., 2002); and similar to the timolol studies, the effect of using a high dose of brimonidine was tested to observe if there would be any changes to drug release profiles with and without the different types of eye movement. Similar to timolol, no significant differences in release profiles were seen between all experimental arms with and without movement. The highest concentrations were seen in the anterior cavity leftover (20.0–60.0 μg/ml) and the AH outflow (5.0–25.0 μg/ml) (Figure 9). Similar amounts of brimonidine were recovered from the lens part (1.0–3.0 μg/ml), iris part (0.2–2.5 μg/ml) and hyaloid membrane (1.0–2.5 μg/ml) compartments. Drug passed the iris-lens barrier into the VH (4.0–12.0 μg/ml), RCS membrane (0.5–1.0 μg/ml) and RCS outflow (<0.2 μg/ml). Brimonidine amounts seen in the back of the eye (*via* the RCS outflow and RCS membrane) by the 2.5-h time point were 0.88 ± 0.11%, 1.28 ± 0.49%, 0.97 ± 0.57%, and 0.84 ± 0.51%, and by the 8-h time point, brimonidine amounts were 0.70 ± 0.21%, 0.94 ± 0.40%, 1.48 ± 1.02%, and 0.76 ± 0.33% with smooth pursuit, microsaccadic, saccadic and no movement respectively. A negligible amount of brimonidine was seen to exit *via* the RCS outflow (~0.01%) and approximately 1–2% of the drug was recorded in all other compartments (except AC cavity, AH outflow and VH) for all movements and control (Figures 9, 10). The half-life values for brimonidine in the AC cavity with smooth pursuit, microsaccades, saccades and control were 323.3 min (k: 0.1286 h^{-1}, R^2: 0.8091), 137.6 min (k: 0.3022 h^{-1}, R^2: 0.756), 182.6 min (k: 0.2277 h^{-1}, R^2: 0.6333) and 304.8 min (k: 0.1364, R^2: 0.8249) respectively (Table 1).

Discussion

There is significant interest in developing anterior formulations to reach the back of the eye. Anterior cavity pharmacokinetic function is important to determine the amount of drug needed to diffuse *via* the iris-lens barrier to help optimise new anterior dosage forms. Since the widespread use of intraocular medicines is so recent, there are no *in vitro* preclinical models described in the pharmacopeia specifically designed to determine intraocular pharmacokinetics, especially mass transfer from the front to the back of the eye. Corneal models represent majority of the anterior segment models and are more established than models for the posterior segment. For example, *in vitro* models using isolated corneal epithelial cells from rabbits (Hornof et al., 2005), preclinical cell culture models (Haghjou et al., 2013) and *ex vivo* preclinical models using isolated tissues have been reported (Missel et al., 2010).

However, the majority of the models do not evaluate anterior cavity pharmacokinetics under aqueous outflow.

Intracameral pharmacokinetics have only been sparsely studied even though it is a crucial parameter to help understand topical drug delivery and different drug delivery systems. Intracameral delivery is a direct method, which has been reported to reduce corneal, conjunctival and systemic side effects, and bypasses the corneal barrier (Shah et al., 2018). Clinically, a sustained release implant of bimatoprost is administered intracamerally to lower the IOP in patients with glaucoma, but may also have neuroprotective effects if suitable posterior segment concentrations can be achieved (Seal et al., 2019). Understanding mass transfer and elimination CL pathways will help develop models appropriate for evaluating intracameral delivery systems. Previous work focused on the development and evolution of a model to accelerate the development of long-acting medicines to the back of the eye (the PK-Eye™), which mimics the mass transfer characteristics caused by anterior aqueous outflow (Awwad et al., 2013; Awwad et al., 2015). It has been shown to give results similar to human CL times from the vitreous cavity for protein therapeutics, non-permeable low molecular weight molecules and peptides from either suspensions or implantable depots (Awwad et al., 2015; Awwad et al., 2017b; Awwad et al., 2018 Egbu et al., 2018). Permeable low molecular weight molecules are eliminated from the vitreous cavity by both the aqueous outflow route and permeation through the retina *via* the RCS pathway (Haghjou et al., 2013; Awwad et al., 2015). The model reported here incorporated different layers to mimic that of the eye, i.e., a silicone cornea, an anterior chamber with TM outflow, an iris part, a lens part, a ciliary flow inlet, hyaloid membrane, VH (with the use of SVF), and RCS membrane with RCS outflow. The AH outflow in the intracameral models broadly mimics the physiological routes of the human eye, with the inlet located at the ciliary body in front of the hyaloid membrane and the outlet right at the base of the anterior chamber through the TM.

Eye rotations reproduced here represent the three main types of ocular movement: fixation with microsaccades, observation of a passing object with the smooth pursuit movement, and finally a rapid and repetitive eye movement in the form of saccades illustrated by reading a book. Moving the model under the current parameters did not seem to affect the CL profiles from the models. This could be due to the fact that eye motions are relatively limited compared to real life where the eye can move along the 3 directions. Only movements along the transverse plane were reproduced and no movements along the sagittal or coronal plane were implemented. In addition, no head movements that could enhance eye movement were included. It can be concluded that the design of the different parts of the model is clearly the key for intracameral modelling while the mechanical eye movements do not seem to affect drug recovery when looking at a completely solubilised drug after intracameral injection.

The intracameral model was used to study the kinetics of two small molecules, timolol and brimonidine, which are used in the clinic for the treatment of glaucoma. Both drugs were evaluated for their release profiles and compared to available pharmacokinetic data in literature. A drug immediately starts to diffuse as soon as it is injected to the target site (Taka et al., 2020). While diffusing in all directions, the drug is also convected at a rate of 2.0 μL/min towards the TM away from the back of the eye. The flow convection tends to prevent the drug from reaching the back of the eye while drug diffusion and an apparent minor contribution from different saccadic motions help the drug to migrate towards the posterior segment. Majority of the drug was seen to remain in the anterior chamber and AH outflow. A slightly higher drug concentration was seen in the VH space in the earlier time points of the low dose studies. Based on the structure of the prototype used, in which fluid flows anteriorly to the membrane, which holds the SVF in place, a fluid "pocket" could have been created between the anterior compartment in front of the lens part and the anterior part of the SVF. Within this pocket, it is expected that convection caused fluid exchange, which equilibrated the drug concentration on either side of the membrane; and because drug injection occurs just behind the lens, a rapid drug movement may have occured into the pocket, causing drug to move into the anterior portion of the SVF. In addition, inhomogeneity of the pocket in the anterior vitreous with the rest of the more viscous posterior SVF and subsequent slow diffusion of drug towards the posterior SVF may have resulted in drug calculations showing higher concentrations in the SVF compared to AH outflow especially in the earlier time points.

To understand the effects of each motion on drug movement, flow convection and drug diffusion can be quantified. While it was difficult to find exact diffusion coefficient factors of these two drugs in the AH, the drug permeability for timolol and brimonidine solutions were found to be similar across porcine corneas with values of $0.75 \pm 0.05 \times 10^{-6}$ and $0.63 \pm 0.05 \times 10^{-6} cm^2/s$ respectively. If similar diffusion coefficients are assumed for both drugs, a value of approximately 10^{-9} cm^2/s (brimonidine has a diffusion factor value of $2.34 \times 10^{-9} cm^2/s$ in water) can be assumed (Lee, 2013). A value of approximately 10^{-5} cm^2/s was obtained when the flow rate of 2.0 μL/min was converted into a fictional diffusion factor (Velentza-Almpani et al., 2022). This fictional diffusion factor is 4 orders of magnitude larger than the diffusion factor of the drugs. It can be assumed that most of the drug will be found in the anterior chamber and AH outflow. The results showed that the drug left in the anterior chamber and AH outflow were 1–2 orders of magnitude larger than most parts of the model. The amount of drug recovery reduced with parts located further back in the eye with the exception of the

iris part of the model with very little drug collected (a natural iris will contain melanin, which can act as an avid drug depot system for some drugs like pilocarpine). The iris part of the model is made of silicone (polysiloxane), a hydrophobic polymer; therefore, it can be expected that hydrophilic drugs like timolol and brimonidine would be repelled by its hydrophobic surface. It can also be noticed that the difference in the amount of drug recovered for each part of the eye is negligible between the different eye movements (maximum velocity of 41°/s) and the static model (no movement).

While the current model broadly accounts for drug CL *via* the AH and RCS outflow, it does not account for iris-ciliary permeation, which would impact CL for molecules with different log *D* values (Fayyaz et al., 2020a; Naageshwaran et al., 2022). Drugs that are more lipophilic are expected to clear faster, for example, a study reported that intracameral dexamethasone (a hydrophobic drug) predominantly cleared *via* the iris-ciliary body as compared to aqueous outflow and corneal permeation in rabbit eyes (Naageshwaran et al., 2022). A similar trend was observed with intracameral timolol, with approximately 16% of the drug eliminating *via* the AH outflow resulting in a half-life of 33.64 min in rabbit eyes (Fayyaz et al., 2020a). Another study suggested the importance of high drug binding of intracameral brinzolamide to tissues, such as, the iris-ciliary body (Naageshwaran et al., 2020). Development of IVIVCs for CL of hydrophobic drugs from the vitreous cavity was previously demonstrated due to the lack of an RCS pathway with the previous PK-Eye™ prototype (Awwad et al., 2017b). *In vitro* data obtained from the model was combined with *in vivo* permeation and CL data to obtain a more realistic prediction of CL from the posterior cavity after intravitreal injection (Awwad et al., 2017b). Similarly, to account for the lack of iris-ciliary permeation, IVIVCs can be developed using AC CL data combined with iris-ciliary permeation *in vivo* data from literature to better estimate drug kinetics of intracameral drugs and formulations after ocular administration.

It is reported that of the 0.07–4% of topically administered drug that reaches the AH, less than 0.001% is recovered from the retina (Loftsson, 2022). Thus, the amount of drug reaching the retina part of the eye is 70 to 4,000× lower than the amount in the AH. Following intracameral injection of brimonidine in the model, approximately 0.41% of the drug reached the retina (RCS outflow and RCS membrane) after 1.5-h with smooth pursuit, a value about 244× lower than the injected amount in the AH. In the case of timolol, about 0.96% of drug was found in the RCS outflow, which was about 2 orders of magnitude lower than the amount in the AH after intracameral injection. While a comparatively larger amount of each drug was able to go through the RCS barrier than typical topical drug delivery, the intracameral model presented here is able to discriminate different drug ocular pathways with negligible amount of drug reaching the blood flow barrier. This demonstrates that it is possible to reproduce complex fluidic pathways in a model for drug delivery to the back of the eye.

Conclusion

The design of an *in vitro* model that studies mass transfer from the anterior to the posterior cavity is reported. The model incorporated aqueous inflow from the ciliary inlet at the physiological flow rate, two CL elimination pathways, human cavity dimensions and a SVF. These results indicate that the model can be used to determine estimates of mass transfer of drugs from the anterior to the posterior segment *via* the iris-lens barrier, and can help in developing intracameral and topical formulations to treat back of the eye diseases.

Data availability statement

The original contributions presented in the study are included in the article/Supplementary Material, further inquiries can be directed to the corresponding authors.

Author contributions

Conceptualisation, YB, SA, PTK, and SB; methodology: TL, SA, and YB; software, SA, TL, and YB; validation, SA, TL, YB, and NI; formal analysis, SA and TL; investigation: TL, SA, YB, and NI; resources, YB, TL, NI, SA, SB, and PTK; data curation, TL, SA, and YB, writing—original draft preparation, SA; writing—review and editing, SA, YB, NI, TL, SB, and PTK; visualisation, YB, TL, SA, NI, SB, and PTK; supervision, SA and YB; project administration, SA and YB; funding acquisition, SA and PTK. All authors have read and agreed to the published version of the manuscript.

Funding

This study received funding from the UK Research and Innovation (Innovate UK Smart Grant, project 41536). TL is grateful for funding from Optceutics Ltd. NI is grateful for funding from Santen Pharmaceuticals Inc, Co. SA, YB, PTK and SB acknowledge the support of UK National Institute for Health Research Biomedical Research Centre at Moorfields Eye Hospital and the UCL Institute of Ophthalmology, the Helen Hamlyn Trust in memory of Paul Hamlyn, the Michael and Isle Katz Foundation, John Nolan and Moorfields Eye Charity. All funders listed were not involved in the study design, collection,

analysis, interpretation of data, the writing of this article or the decision to submit it for publication. All authors declare no other competing interests.

Conflict of interest

SA, SB and PTK are co-founders of Optceutics Ltd. Improvements and design changes to the models are described in a patent specification (Awwad et al., 2021), which lists SA, YB, NI, SB and PTK as co-inventors.

The remaining author declares that the research was conducted in the absence of any commercial or financial relationships that could be construed as a potential conflict of interest.

Publisher's note

Supplementary material

The Supplementary Material for this article can be found online at: https://www.frontiersin.org/articles/10.3389/fddev.2022.1025029/full#supplementary-material

References

Acheampong, A. A., Shackleton, M., John, B., Burke, J., Wheeler, L., and Tang-Liu, D. (2002). Distribution of brimonidine into anterior and posterior tissues of monkey, rabbit, and rat eyes. *Drug Metab. Dispos.* 30 (4), 421–429. doi:10.1124/dmd.30.4.421

Adrianto, M. F., Annuryanti, F., Wilson, C. G., Sheshala, R., and Thakur, R. R. S. (2022). *In vitro* dissolution testing models of ocular implants for posterior segment drug delivery. *Drug Deliv. Transl. Res.* 12, 1355–1375. doi:10.1007/s13346-021-01043-z

Auel, T., Großmann, L., Schulig, L., Weitschies, W., and Seidlitz, A. (2021). The EyeFlowCell: Development of a 3D-printed dissolution test setup for intravitreal dosage forms. *Pharmaceutics* 13 (9), 1394–1414. doi:10.3390/pharmaceutics13091394

Awwad, S., Abubakre, A., Angkawinitwong, U., Khaw, P. T., and Brocchini, S. (2019). *In situ* antibody-loaded hydrogel for intravitreal delivery. *Eur. J. Pharm. Sci.* 137, 104993. doi:10.1016/j.ejps.2019.104993

Awwad, S., Al-Shohani, A., Khaw, P. T., and Brocchini, S. (2018). Comparative study of *in situ* loaded antibody and PEG-fab NIPAAM gels. *Macromol. Biosci. [Internet]* 18 (2), 1–12. doi:10.1002/mabi.201700255

Awwad, S., Bouremel, Y., Ibeanu, N., Brocchini, S. J., and Khaw, P. T (2021). Artificial eye assembly for studying ocular pharmacokinetics. WO 2021/186191. Available at: https://patentscope.wipo.int/search/en/detail.jsf?docId=WO2021186191&tab=PCTBIBLIO&_cid=P20-KTWYO1-27725-1.

Awwad, S., Day, R. M., Khaw, P. T., Brocchini, S., and Fadda, H. M. (2017). Sustained release ophthalmic dexamethasone: *In vitro in vivo* correlations derived from the PK-eye. *Int. J. Pharm.* 522, 119–127. doi:10.1016/j.ijpharm.2017.02.047

Awwad, S., Henein, C., Ibeanu, N., Khaw, P. T., and Brocchini, S. (2020). Preclinical challenges for developing long acting intravitreal medicines. *Eur. J. Pharm. Biopharm.* 153, 130–149. doi:10.1016/j.ejpb.2020.05.005

Awwad, S., Lockwood, A., Brocchini, S., and Khaw, P. T. (2015). The PK-eye: A novel *in vitro* ocular flow model for use in preclinical drug development. *J. Pharm. Sci.* 104 (10), 3330–3342. doi:10.1002/jps.24480

Awwad, S., Lockwood, A., Mohamed Ahmed, A., Sharma, G., Khalili, A., Brocchini, S., et al. (2013). Development of an *in vitro* pharmacokinetic model of the human eye. *Invest. Ophthalmol. Vis. Sci.* 54 (15), 5068.

Awwad, S., Mohamed Ahmed, A. H. A., Sharma, G., Heng, J. S., Khaw, P. T., Brocchini, S., et al. (2017). Principles of pharmacology in the eye. *Br. J. Pharmacol.* 174, 4205–4223. doi:10.1111/bph.14024

Bakri, S. J., Snyder, M. R., Reid, J. M., Pulido, J. S., Ezzat, M. K., and Singh, R. J. (2007). Pharmacokinetics of intravitreal ranibizumab (Lucentis). *Ophthalmology* 114 (12), 2179–2182. doi:10.1016/j.ophtha.2007.09.012

Bastawrous, A., Burgess, P. I., Mahdi, A. M., Kyari, F., Burton, M. J., and Kuper, H. (2014). Posterior segment eye disease in sub-Saharan Africa: Review of recent population-based studies. *Trop. Med. Int. Health* 19 (5), 600–609. doi:10.1111/tmi.12276

Bouremel, Y., Henein, C., and Khaw, P. T. (2021). "Ocular rigidity and surgery," in *Ocular rigidity, biomechanics and hydrodynamics of the eye*. Editors I. Pallikaris, M. K. Tsilimbaris, and A. I. Dastiridou (Berlin, Germany: Springer), 335–359.

Burton, M. J., Ramke, J., Marques, A. P., Bourne, R. R. A., Congdon, N., Jones, I., et al. (2021). The lancet global health commission on global eye health: Vision beyond 2020. *Lancet. Glob. Health* 9 (4), e489–e551. doi:10.1016/S2214-109X(20)30488-5

Chi, Z., Azhar, I., Khan, H., Yang, L., and Feng, Y. (2019). Automatic dissolution testing with high-temporal resolution for both immediate-release and fixed-combination drug tablets. *Sci. Rep.* 9 (1), 17114–17211. doi:10.1038/s41598-019-53750-w

Cunha-Vaz, J. G. (1997). The blood-ocular barriers: Past, present, and future. *Doc. Ophthalmol.* 93 (1–2), 149–157. doi:10.1007/BF02569055

del Amo, E. M., Hammid, A., Tausch, M., Toropainen, E., Sadeghi, A., Valtari, A., et al. (2022). Ocular metabolism and distribution of drugs in the rabbit eye: Quantitative assessment after intracameral and intravitreal administrations. *Int. J. Pharm.* 613, 121361. doi:10.1016/j.ijpharm.2021.121361

Delplace, V., Payne, S., and Shoichet, M. (2015). Delivery strategies for treatment of age-related ocular diseases: From a biological understanding to biomaterial solutions. *J. Control. Release* 219, 652–668. doi:10.1016/j.jconrel.2015.09.065

Egbu, R., Brocchini, S., Khaw, P. T., and Awwad, S. (2018). Antibody loaded collapsible hyaluronic acid hydrogels for intraocular delivery. *Eur. J. Pharm. Biopharm.* 124, 95–103. doi:10.1016/j.ejpb.2017.12.019

Fayyaz, A., Ranta, V. P., Toropainen, E., Vellonen, K. S., Ricci, G. D. A., Reinisalo, M., et al. (2020a). Ocular intracameral pharmacokinetics for a cocktail of timolol, betaxolol, and atenolol in rabbits. *Mol. Pharm.* 17 (2), 588–594. doi:10.1021/acs.molpharmaceut.9b01024

Fayyaz, A., Ranta, V. P., Toropainen, E., Vellonen, K. S., Valtari, A., Puranen, J., et al. (2020b). Topical ocular pharmacokinetics and bioavailability for a cocktail of atenolol, timolol and betaxolol in rabbits. *Eur. J. Pharm. Sci.* 155, 105553. doi:10.1016/j.ejps.2020.105553

Gu, D., and Janetos, T. M. (2021). Ophthalmic drug discovery in the United States over the past two decades. *Ophthalmic Epidemiol.* 28 (1), 21–26. doi:10.1080/09286586.2020.1786591

Haghjou, N., Abdekhodaie, M. J., and Cheng, Y-L. (2013). Retina-choroid-sclera permeability for ophthalmic drugs in the vitreous to blood direction: Quantitative assessment. *Pharm. Res.* 30 (1), 41–59. doi:10.1007/s11095-012-0847-9

Hay, M., Thomas, D. W., Craighead, J. L., Economides, C., and Rosenthal, J. (2014). Clinical development success rates for investigational drugs. *Nat. Biotechnol.* 32 (1), 40–51. doi:10.1038/nbt.2786

Hornof, M., Toropainen, E., and Urtti, A. (2005). Cell culture models of the ocular barriers. *Eur. J. Pharm. Biopharm.* 60 (2), 207–225. doi:10.1016/j.ejpb.2005.01.009

Jager, R. D., Aiello, L. P., Patel, S. C., and Cunningham, E. T. (2004). Risks of intravitreous injection: A comprehensive review. *Retina* 24 (5), 676–698. doi:10.1097/00006982-200410000-00002

Kaitin, K. I., and Dimasi, J. A. (2011). Pharmaceutical innovation in the 21st century: New drug approvals in the first decade, 2000-2009. *Clin. Pharmacol. Ther.* 89 (2), 183–188. doi:10.1038/clpt.2010.286

Kim, H., Csaky, K., Chan, C., Bungay, P., Lutz, R. J., Dedrick, R. L., et al. (2006). The pharmacokinetics of rituximab following an intravitreal injection. *Exp. Eye Res.* 82, 760–766. doi:10.1016/j.exer.2005.09.018

Kuentz, M. (2015). Analytical technologies for real-time drug dissolution and precipitation testing on a small scale. *J. Pharm. Pharmacol.* 67 (2), 143–159. doi:10.1111/jphp.12271

Larsby, B., Thell, J., Möller, C., and Odkvist, L. (1988). The effect of stimulus predictability and age on human tracking eye movements. *Acta Otolaryngol.* 105 (1–2), 21–30. doi:10.3109/00016488809119441

Laude, A., Tan, L. E., Wilson, C. G., Lascaratos, G., Elashry, M., Aslam, T., et al. (2010). Intravitreal therapy for neovascular age-related macular degeneration and inter-individual variations in vitreous pharmacokinetics. *Prog. Retin. Eye Res.* 29 (6), 466–475. doi:10.1016/j.preteyeres.2010.04.003

Lee, J. H. (2013). *Drug delivery microdevice: Design, simulation and experiments*. Richmond, Virginia: Virginia Commonwealth University.

Loch, C., Bogdahn, M., Stein, S., Nagel, S., Guthoff, R., Weitschies, W., et al. (2014). Simulation of drug distribution in the vitreous body after local drug application into intact vitreous body and in progress of posterior vitreous detachment. *J. Pharm. Sci.* 103 (2), 517–526. doi:10.1002/jps.23808

Loftsson, T. (2022). Topical drug delivery to the retina: Obstacles and routes to success. *Expert Opin. Drug Deliv.* 19 (1), 9–21. doi:10.1080/17425247.2022.2017878

Meyer, C. H., Lasker, A. G., and Robinson, D. A. (1985). The upper limit of human smooth pursuit velocity. *Vis. Res.* 25 (4), 561–563. doi:10.1016/0042-6989(85)90160-9

Missel, P., Chastain, J., Mitra, A., Kompella, U., Kansara, V., Duvvuri, S., et al. (2010). *In vitro* transport and partitioning of AL-4940, active metabolite of angiostatic agent anecortave acetate, in ocular tissues of the posterior segment. *J. Ocul. Pharmacol. Ther.* 26 (2), 137–146. doi:10.1089/jop.2009.0132

Naageshwaran, V., Ranta, V. P., Gum, G., Bhoopathy, S., Urtti, A., and del Amo, E. M. (2020). Comprehensive ocular and systemic pharmacokinetics of brinzolamide in rabbits after intracameral, topical, and intravenous administration. *J. Pharm. Sci.* 110, 529–535. doi:10.1016/j.xphs.2020.09.051

Naageshwaran, V., Ranta, V. P., Toropainen, E., Tuomainen, M., Gum, G., Xie, E., et al. (2022). Topical pharmacokinetics of dexamethasone suspensions in the rabbit eye: Bioavailability comparison. *Int. J. Pharm.* 615, 121515. doi:10.1016/j.ijpharm.2022.121515

Patel, S., Müller, G., Stracke, J. O., Altenburger, U., Mahler, H-C., and Jere, D. (2015). Evaluation of protein drug stability with vitreous humor in a novel *ex-vivo* intraocular model. *Eur. J. Pharm. Biopharm.* 95, 407–417. doi:10.1016/j.ejpb.2015.04.033

Rayner, K. (1998). Eye movements in reading and information processing: 20 years of research. *Psychol. Bull.* 124 (3), 372–422. doi:10.1037/0033-2909.124.3.372

Sapino, S., Peira, E., Chirio, D., Chindamo, G., Guglielmo, S., Oliaro-Bosso, S., et al. (2019). Thermosensitive nanocomposite hydrogels for intravitreal delivery of cefuroxime. *Nanomaterials* 9 (10), 1461. doi:10.3390/nano9101461

Schopf, L. R., Popov, A. M., Enlow, E. M., Bourassa, J. L., Ong, W. Z., Nowak, P., et al. (2015). Topical ocular drug delivery to the back of the eye by mucus-penetrating particles. *Transl. Vis. Sci. Technol.* 4, 11–12. doi:10.1167/tvst.4.3.11

Seal, J. R., Robinson, M. R., Burke, J., Bejanian, M., Coote, M., and Attar, M. (2019). Intracameral sustained-release bimatoprost implant delivers bimatoprost to target tissues with reduced drug exposure to off-target tissues. *J. Ocul. Pharmacol. Ther.* 35 (1), 50–57. doi:10.1089/jop.2018.0067

Shah, T. J., Conway, M. D., and Peyman, G. A. (2018). Intracameral dexamethasone injection in the treatment of cataract surgery induced inflammation: Design, development, and place in therapy. *Clin. Ophthalmol.* 12, 2223–2235. doi:10.2147/OPTH.S165722

Shatz, W., Hass, P. E., Mathieu, M., Kim, H. S., Leach, K., Zhou, M., et al. (2016). Contribution of antibody hydrodynamic size to vitreal clearance revealed through rabbit studies using a species-matched fab. *Mol. Pharm.* 13 (9), 2996–3003. doi:10.1021/acs.molpharmaceut.6b00345

Shen, J., Moats, R. A., Pollack, H. A., Robinson, M. R., and Attar, M. (2020). Distribution of 14C-latanoprost following a single intracameral administration versus repeated topical administration. *Ophthalmol. Ther.* 9 (4), 929–940. doi:10.1007/s40123-020-00285-3

Taka, E., Karavasili, C., Bouropoulos, N., Moschakis, T., Andreadis, D. D., Zacharis, C. K., et al. (2020). Ocular co-delivery of timolol and brimonidine from a self-assembling peptide hydrogel for the treatment of glaucoma: *In vitro* and *ex vivo* evaluation. *Pharmaceuticals* 13 (6), 1266–E213. doi:10.3390/ph13060126

Thakur, S. S., Shenoy, S. K., Suk, J. S., Hanes, J. S., and Rupenthal, I. D. (2020). Validation of hyaluronic acid-agar-based hydrogels as vitreous humor mimetics for *in vitro* drug and particle migration evaluations. *Eur. J. Pharm. Biopharm.* 148, 118–125. doi:10.1016/j.ejpb.2020.01.008

Urtti, A., Pipkin, J. D., Rork, G., Sendo, T., Finne, U., and Repta, A. J. (1990). Controlled drug delivery devices for experimental ocular studies with timolol 2. Ocular and systemic absorption in rabbits. *Int. J. Pharm. X.* 61 (3), 241–249. doi:10.1016/0378-5173(90)90215-p

Velentza-Almpani, A., Ibeanu, N., Liu, T., Redhead, C., Khaw, P. T., Brocchini, S., et al. (2022). Effects of flow hydrodynamics and eye movements on intraocular drug clearance. *Pharmaceutics* 14 (6), 1267. doi:10.3390/pharmaceutics14061267

Yi, H., Feng, Y., and Gappa-Fahlenkamp, H. (2022). Analysis of topical dosing and administration effects on ocular drug delivery in a human eyeball model using computational fluid dynamics. *Comput. Biol. Med.* 141, 105016. doi:10.1016/j.compbiomed.2021.105016